Efficient Low Bandgap Polymer Solar Cell with Ordered Heterojunction Defined by Nanoimprint Lithography

ARTICLE *in* ACS APPLIED MATERIALS & INTERFACES · OCTOBER 2014

Impact Factor: 6.72 · DOI: 10.1021/am505303a · Source: PubMed

4 AUTHORS:

Yi Yang
GlobalFoundries Inc.
5 PUBLICATIONS **102** CITATIONS
SEE PROFILE

Kamil Mielczarek
University of Texas at Dallas
23 PUBLICATIONS **333** CITATIONS
SEE PROFILE

Anvar A. Zakhidov
University of Texas at Dallas
62 PUBLICATIONS **242** CITATIONS
SEE PROFILE

Walter Hu
University of Texas at Dallas
143 PUBLICATIONS **1,574** CITATIONS
SEE PROFILE

ACS APPLIED MATERIALS & INTERFACES

Research Article

www.acsami.org

Efficient Low Bandgap Polymer Solar Cell with Ordered Heterojunction Defined by Nanoimprint Lithography

Yi Yang,[†] Kamil Mielczarek,[‡] Anvar Zakhidov,[†,‡] and Walter Hu*[,†,§]

[†]Department of Materials Science and Engineering, [‡]Department of Physics, [§]Department of Electrical Engineering, The University of Texas at Dallas, Richardson, Texas 75080, United States

ABSTRACT: In this work, we demonstrate the feasibility of using nanoimprint lithography (NIL) to make efficient low bandgap polymer solar cells with well-ordered heterojunction. High quality low bandgap conjugated polymer poly[2,6-(4,4-bis(2-ethylhexyl)-4H-cyclopenta[2,1-b;3,4-b′]-dithiophene)-*alt*-4,7-(2,1,3-benzothiadiazole)] (PCPDTBT) nanogratings are fabricated using this technique for the first time. The geometry effect of PCPDTBT nanostructures on the solar cell performance is investigated by making PCPDTBT/C_{70} solar cells with different feature sizes of PCPDTBT nanogratings. It is found that the power conversion efficiency (PCE) increases with increasing nanograting height, PCPDTBT/C_{70} junction area, and decreasing nanograting width. We also find that NIL makes PCPDTBT chains interact more strongly and form an improved structural ordering. Solar cells made on the highest aspect ratio PCPDTBT nanostructures are among the best reported devices using the same material with a PCE of 5.5%.

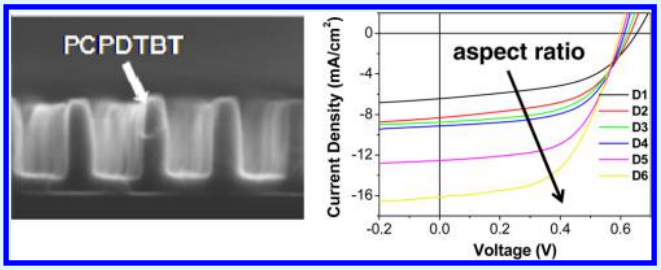

KEYWORDS: *morphology of polymer solar cell, nanoimprint lithography, ordered heterojunction, chain ordering, nanostructure geometry effect*

1. INTRODUCTION

In recent years, polymer solar cells have drawn considerable amounts of research interest due to their attractive features including flexibility, semitransparency, and manufacturability using cost-effective continuous printing processes.[1,2] However, one challenge limiting their commercialization is the relatively low power conversion efficiency (PCE) when compared to their inorganic counterparts. One of the causes for their low performance is the difficulty to simultaneously realize donor−acceptor phase separation within the short exciton diffusion length (∼10 nm) and high charge mobility, especially hole mobility, which are critical for charge separation and transport.[3,4] The bulk heterojunction (BHJ) has shown promise to solve these two issues through its large donor−acceptor interface area as well as thermal or solvent vapor annealing assisted polymer crystallization.[5−7] However, the active layer morphology in this structure cannot be precisely controlled. Significant charge recombination is caused by discrete and randomly distributed phases, resulting in inefficient charge separation and transport.[8] Nowadays, nanoimprint lithography (NIL) has emerged as an effective fabrication technique to precisely define the nanomorphology in polymer solar cells.[9] Controlled chain ordering as well as a bicontinuous and interdigitized heterojunction can be achieved by imprinting conjugated polymers, where a nanoimprint induced chain alignment is present, followed by infiltrating fullerene into patterned polymer nanostructures.[10−17] However, it is noted that, in literature, most studies are focused on nanoimprinted poly(3-hexylthiophene-2,5-diyl) (P3HT)/fullerene solar cells, the most studied material combination.[10,13,14,16,18−22] This combination is not ideal due to a mismatch between the absorption of P3HT and solar spectrum, which has a maximum photon flux at 1.6−1.8 eV while P3HT has a relatively large bandgap of 1.9−2.0 eV. Therefore, a bandgap of 1.3−1.5 eV is considered to be ideal for polymer−fullerene solar cells.[23] In recent years many low bandgap polymers have been synthesized with record-breaking efficiencies.[24−27] However, it has been proven that the donor and acceptor phase separation for these polymers cannot be realized by thermal or solvent vapor annealing, which is usually carried out on P3HT/fullerene solar cells.[7,28,29] Although additives such as 1,8-octanedithiol are added into the solution to help separate donor and acceptor domains, this separation cannot be controlled precisely.[28,30−33] Therefore, NIL would provide an effective solution if an ordered active layer morphology could be formed by it. However, no work has been reported thus far and it remains unknown if NIL can be applied to a wide variety of materials in the polymer solar cell field. Moreover, inconsistent geometries of imprinted polymer nanostructures have been used by different groups, which result in different PCEs.[13,14,18,21,34,35] It is therefore difficult to compare the results of one work to another. A systematical study on the correlation between nanostructure geometry and device performance is needed to unleash the full potential of this

Received: August 7, 2014
Accepted: October 8, 2014

   dx.doi.org/10.1021/am505303a | *ACS Appl. Mater. Interfaces* XXXX, XXX, XXX−XXX

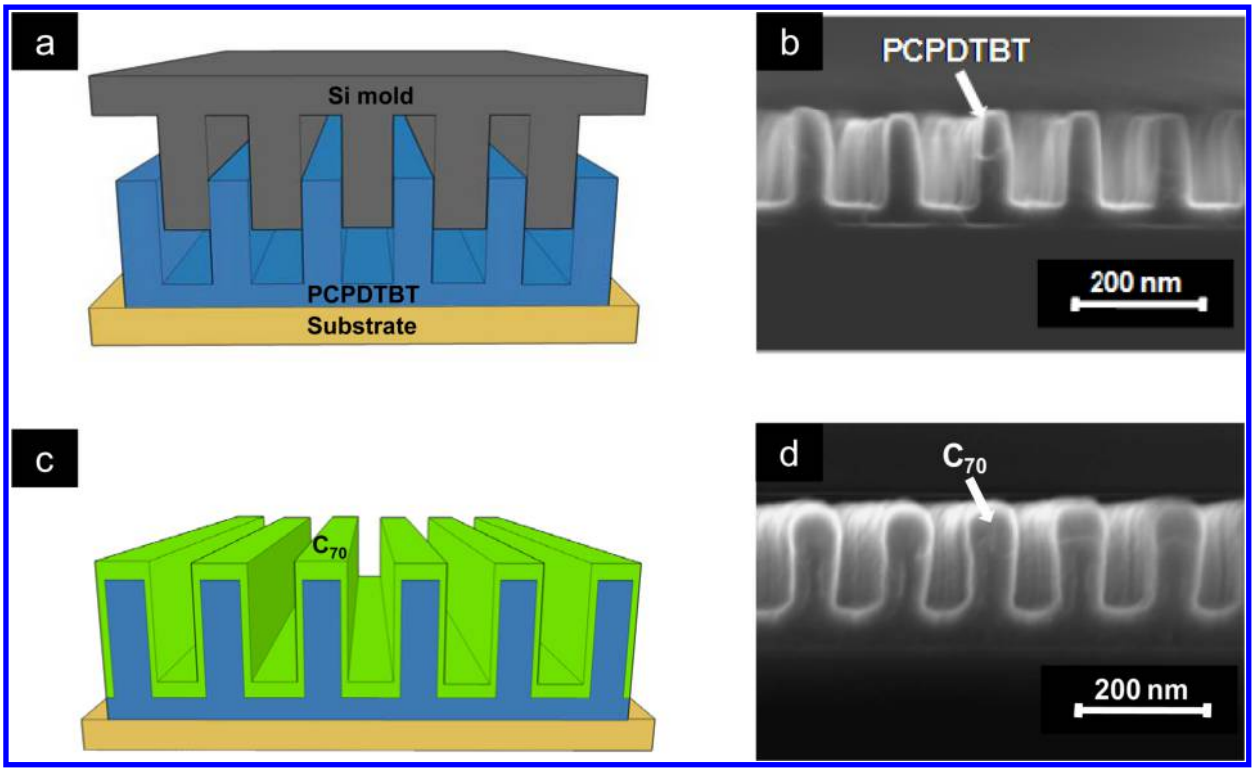

Figure 1. Process flow to form ordered PCPDTBT/C_{70} heterojunction: (a and b) NIL of PCPDTBT nanogratings; (c and d) complete coverage of C_{70} on top of PCPDTBT nanogratings.

Table 1. Summary of PCPDTBT Nanogratings with Different Geometries

geometry (G) no.	1	2	3	4	5	6
width/spacing (nm)		280/280	210/210	60/80	60/80	60/80
height (nm)	70 (thin film)	110	110	50	110	170
residual layer (nm)		20	20	20	20	20
IEF (A/A_0)	1	1.39	1.52	1.71	2.57	3.43

emerging technique toward significant improvement of polymer solar cell performance. Whether there is any NIL improved chain ordering for these materials is worth investigating as well.

In this work, we have utilized NIL to pattern the low bandgap (1.4 eV) solar cell polymer, poly[2,6-(4,4-bis(2-ethylhexyl)-4H-cyclopenta[2,1-b;3,4-b′]-dithiophene)-*alt*-4,7-(2,1,3-benzothiadiazole)] (PCPDTBT).[25,27,28,30] High quality nanogratings for this polymer are achieved using this technique for the first time. We then study the nanostructure geometry effect on the solar cell performance by making PCPDTBT/C_{70} solar cells on nanogratings with consistently varied widths and heights. It is found that the performance increases with increasing nanograting height, PCPDTBT/C_{70} junction area, and decreasing nanograting width. We also find that NIL makes PCPDTBT chains interact more strongly and form an improved structural ordering. Solar cells with the narrowest and highest PCPDTBT nanogratings among all devices give the optimal PCE of 5.5%, which is among the best efficiencies reported for this polymer in literature.

2. EXPERIMENTAL SECTION

2.1. Nanoimprint Lithography and UV−Vis Measurement of PCPDTBT Nanogratings. To fabricate nanogratings, PCPDTBT (1-Material, Inc.) solution was first prepared in chlorobenzene and then spin-coated onto substrates (Si or glass). As described in our previous study, the polymer has to be mechanically strong if one wants to fabricate high aspect ratio (AR) nanostructures by NIL.[36] To test this polymer, a Si mold with the highest AR (~2.83) we could make with width w = 80 nm, spacing p = 60 nm, and height h = 170 nm was used initially. The mold was treated with 1H,1H,2H,2H-perfluorodecyltrichlorosilane (FDTS) as an antiadhesion coating.[37] NIL was performed at a temperature of 170 °C and a pressure of 5 MPa for 10 min. Then, the system was cooled slowly to 70 °C, and the mold was released from the substrates. The schematic of imprint process is shown in Figure 1a. Figure 1b shows that high quality PCPDTBT nanogratings were fabricated from the Si mold with excellent fidelity, which made it possible to fabricate solar cells with these nanostructures. To study if there was any NIL improved chain ordering, NIL formed nanogratings were characterized by UV−vis measurement (Agilent 8453 spectrometer), a common method for this polymer.[27,28,30] It should be noted that in this study we also tried X-ray diffraction, which is usually employed to study the chain alignment in polymers such as P3HT in literature. However, it was found that this characterization approach did not work well for this low crystallinity polymer because it could not generate high and sharp peaks on the X-ray spectra and made result analysis difficult. UV−vis measurement is more sensitive to the structure change in this type of polymer, as elaborated in the literature.[28]

In this work, the geometry of PCPDTBT nanogratings were consistently varied to study its effects on solar cell performance, as summarized in Table 1. It should be noted that G1, 70 nm flat thin film, was used as reference and approximately the same thickness as G2 (w = 280 nm, p = 280 nm, and h = 110 nm), G3 (w = 210 nm, p = 210 nm, and h = 110 nm), and G5 (w = 60 nm, p = 80 nm, and h = 110 nm) before they were imprinted into nanostructures. Moreover in

dx.doi.org/10.1021/am505303a | ACS Appl. Mater. Interfaces XXXX, XXX, XXX−XXX

all experiments of this work, the flat thin film G1 was imprinted by a flat mold at the same temperature and pressure as nanostructured samples. The residual layer was 20 nm and constant for all geometries. The imprinted nanogratings increase the interface area of heterojunction from the bilayer structure, which can be quantified using a term named interface enhancement factor (IEF) in eq 1. IEF describes the ratio of imprinted nanostructure interface area (A) to non-imprinted or the initial area before imprinting.[13]

$$\mathrm{IEF} = A/A_0 = 1 + \frac{2h}{w + p} \quad (1)$$

It constantly increased from G1 to G6 as listed in Table 1. In this work we could not increase the IEF any further due to our limitations on mold fabrication and demolding process after NIL.

2.2. Solar Cell Fabrication and Characterization. Solar cells were fabricated using imprinted PCPDTBT nanogratings in the following structure: ITO/PEDOT:PSS/PCPDTBT/C_{70}/Al. First a thin layer (~20 nm) of PEDOT:PSS (CLEVIOS P VP Al 4083, H. C. Starck, Inc.) was spin-coated onto patterned ITO coated glass substrates (Luminescence Technology) and baked at 150 °C for 15 min. In this work, low conductive PEDOT:PSS was chosen to minimize the measurement error from device areas due to the lateral conductivity of PEDOT:PSS. Then, PCPDTBT thin films were spin-coated and imprinted by nanograting molds with different feature sizes to form different geometries under the above temperature and pressure. After NIL, an optimized layer of C_{70} (Nano-C, Ltd.) with a thickness of 50 nm was thermally evaporated onto the PCPDTBT nanostructures at the rate of 0.5 Å/s, as shown in Figure 1c. To improve the C_{70} coverage onto PCPDTBT nanogratings, a rotational deposition method was introduced, which thermally evaporated C_{70} from all directions at a fixed angle of 20°. Figure 1d shows that a complete coverage of C_{70} onto the imprinted PCPDTBT nanogratings was realized. In this work, spin-coating of the widely used acceptors [6,6]-Phenyl-C61-butyric acid methyl ester ($PC_{61}BM$) or $PC_{71}BM$ was not chosen because there is no orthogonal solvent available. Moreover, C_{70} has a stronger absorbance compared to C_{60} due to its asymmetric structure and can thus form a complementary absorption range with PCPDTBT, similar to $PC_{71}BM$.[38] Finally, 100 nm Al was deposited obliquely on top as the cathode by thermal evaporation. In this work, we could not obtain a clear image after Al deposition because the cross-section consisting of multiple layers can be easily damaged during sample preparation. However, we can confirm that the contact between Al and active layer is well formed from the high PCE (5.5%) generated from these devices. Otherwise, the PCE would be very poor if there was an infiltration issue as we observed before. For bilayer solar cells in literature, people usually thermally anneal devices so that the donor and acceptor can diffuse into each other, form a larger interface and increase PCE. However, in our work thermal annealing was avoided because we wanted to precisely control the interface area between PCPDTBT and C_{70} so that the geometry effect of imprinted nanostructures on solar cell performance could be studied. Four solar cell pixels were formed on each substrate with an active area of 3 × 3 mm^2 each. To improve the reproducibility and accuracy, all devices were well masked to minimize the shadow and edge effects before measurement. The current density−voltage (J−V) characteristics were measured using Air Mass 1.5 global solar simulated light (AM. 1.5G) calibrated using an NREL traceable KG5 color filtered silicon photodiode (PV Measurements Inc.) to an intensity of 100 mW/cm^2. To reduce the experimental errors, ten batches of solar cells were made in this work. The average and standard deviation of device characteristics were calculated from these ten batches (10 × 4 devices in total for each geometry).

3. RESULTS AND DISCUSSION

The J−V characteristics of these solar cells are shown in Figure 2. Open circuit voltage (V_{oc}), short circuit current (J_{sc}), fill factor (FF), and PCE of these devices are extracted from the J−V curves and listed in Table 2. The overall dependence of these

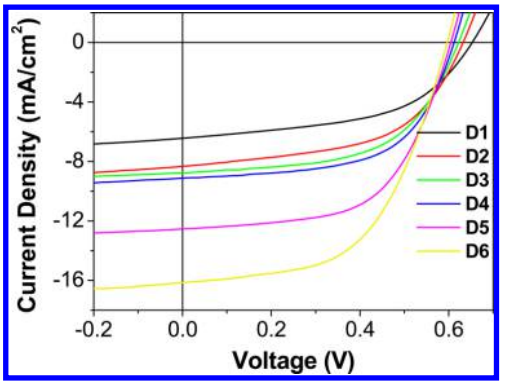

Figure 2. J−V characteristics of PCPDTBT/C_{70} solar cells fabricated with different PCPDTBT geometries: 70 nm flat thin film (D1), nanogratings with width and height of 280 and 110 nm (D2), 210 and 110 nm (D3), 60 and 50 nm (D4), 60 and 110 nm (D5), and 60 and 170 nm (D6), respectively.

device characteristics on the nanostructure width, height, and IEF are illustrated in Figure 3. It is found that the J_{sc} and FF of these devices are highly dependent on the nanograting geometry. Let us first discuss the geometry effect on J_{sc}. As shown in Figure 2 and 3a, when compared to D1, D2, D3, and D5, which have the same height, show improved J_{sc}. Moreover among D2, D3, and D5, J_{sc} increases constantly with the decrease of nanograting width. This is expected because smaller widths of nanostructures with the same height would result in bigger interface area, or larger IEF according to eq 1. When the nanostructure width gets smaller, that is, closer to the exciton diffusion length, charge separation can be improved. For devices D4, D5, and D6 with the same width/spacing (60 nm/80 nm) but increasing height from 50 nm, 110 to 170 nm, we observe an increase in J_{sc} with increasing nanostructure height. Similarly, this is expected as increasing height would result in larger IEF, and also better light absorption in the higher nanostructures.

When it goes to the geometry effect on FF, Table 2 and Figure 3b have shown that there is a constant increase of FF with decreasing nanostructure width and the same height, that is, from FF = 0.51 for flat thin film device D1, FF = 0.55 for D2 when w = 280 nm, FF = 0.56 for D3 when w = 210 nm, to FF= 0.58 for D5 when w = 60 nm. FF is dependent on many factors such as charge carrier mobility, charge collection efficiency and charge recombination rate. It should be noted that in this work, C_{70} is deposited onto different sizes of PCPDTBT nanogratings in the same way to study the nanostructure geometry effect. This results in different C_{70} coverages for these devices, making it difficult to separate the effects of above factors from each other. Therefore, it is challenging to find all possible reasons for these changes, and here, we only aim to find part of them. In literature, people have found that the improved FF is due to the enhanced chain ordering for imprinted P3HT nanostructures.[11,19−21,39] Here, we speculate that these changes in FF might be partially explained by the same reason. As we introduce in the Experimental Section, X-ray diffraction is not a proper tool to confirm this due to the low crystallinity of PCPDTBT. Instead it can be characterized by the absorption measurement, that is, an improved chain ordering of this polymer is usually associated with a red-shift on the absorbance spectra, as suggested in literature.[27,28] There is a concern that the periodic structures of imprinted nanogratings, which are within the wavelength of visible light, might affect the spectra

dx.doi.org/10.1021/am505303a | ACS Appl. Mater. Interfaces XXXX, XXX, XXX−XXX

Table 2. Performance of PCPDTBT/C_{70} Photovoltaic Devices Built on PCPDTBT Nanogratings with Different Geometries

	D1	D2	D3	D4	D5	D6
width/spacing/height (nm)	70 nm thin film	280/280/110	210/210/110	60/80/50	60/80/110	60/80/170
IEF = A/A_0	1	1.39	1.52	1.71	2.57	3.43
V_{oc} (V)	0.65 ± 0.01	0.63 ± 0.01	0.62 ± 0.01	0.61 ± 0.01	0.60 ± 0.01	0.59 ± 0.01
J_{sc} (mA/cm^2)	6.43 ± 0.39	8.33 ± 0.28	8.79 ± 0.36	9.12 ± 0.49	12.54 ± 0.66	16.15 ± 0.63
FF	0.51 ± 0.01	0.55 ± 0.01	0.56 ± 0.01	0.59 ± 0.01	0.58 ± 0.01	0.58 ± 0.01
PCE (%)	2.13 ± 0.17	2.89 ± 0.13	3.05 ± 0.15	3.28 ± 0.24	4.36 ± 0.27	5.52 ± 0.31

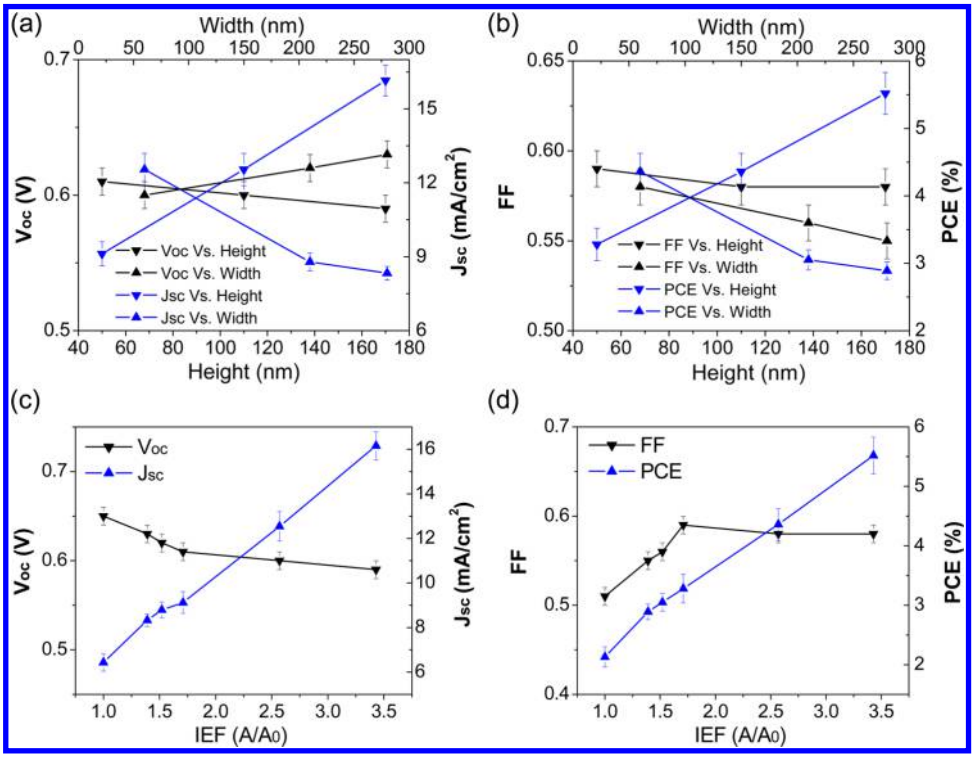

Figure 3. PCPDTBT nanograting geometry effect on the PCPDTBT/C_{70} solar cell performance: (a, b) the width/height, and (c, d) IEF (A/A_0) effects on V_{oc}, J_{sc}, (a, b) FF and PCE (c, d), respectively.

due to optical effects such as scattering and diffraction. However, one can determine whether there is NIL improved chain ordering from the V_{oc} as well. If the chain ordering really occurs, it would increase the highest occupied molecular orbital (HOMO) level of PCPDTBT to narrow its effective bandgap, and thus reduce the V_{oc}, because V_{oc} is scale with the difference between the HOMO of the donor and the lowest unoccupied molecular orbital (LUMO) of the acceptor materials.[28,40] As shown in Figure 4, compared to G1, G2 and G3 show red-shifts and broader absorption shoulders and these changes are the largest at G5. Furthermore, there is a constant decrease of V_{oc} from D1 to D5, that is, from 0.65 V for D1, 0.63 V for D2, 0.62 V for D3, and 0.60 V for D5. Therefore, these findings together suggest that the polymer chains interact more strongly and form an improved structural ordering when PCPDTBT nanostructure width decreases. It is consistent with the trend of FF and thus provides a preliminary evidence to our speculation. We believe one possible explanation of this trend is that when these samples are imprinted by molds with decreasing widths but the same height, the total interface area between the polymer and molds becomes larger (higher IEF). This larger interface area enables a stronger polymer-to-mold interaction, which has been proven to be one of the origins of chain ordering in literature.[41−43] Here, we plot the peak

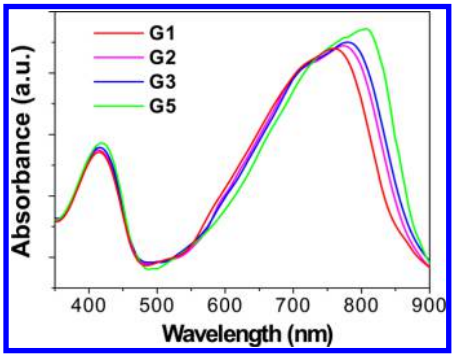

Figure 4. Light absorbance of PCPDTBT samples with different geometries: 70 thin film (G1), nanogratings with width w = 280 nm and height h = 110 nm (G2), w = 210 nm and h = 110 nm (G3), and w = 60 nm and h = 110 nm (G5).

wavelength of PCPDTBT absorbance spectra for these geometries as a function of IEF. As shown in Figure 5, the NIL induced increase in peak wavelength changes almost linearly with IEF, which proves our speculation preliminarily. This enhanced chain ordering also adds one explanation why J_{sc} constantly increases with decreasing nanostructure width as observed in Figure 3a.

dx.doi.org/10.1021/am505303a | ACS Appl. Mater. Interfaces XXXX, XXX, XXX−XXX

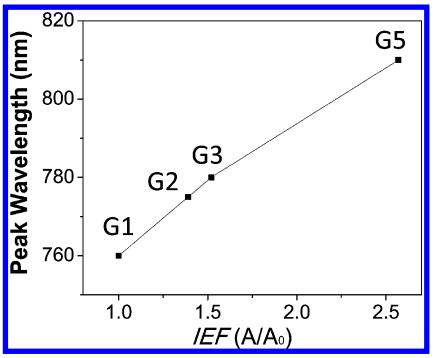

Figure 5. Effects of IEF (A/A_0) on the peak wavelength of PCPDTBT absorbance spectra for geometries G1, G2, G3, and G5.

Among all the devices we have made, device D6 with the smallest nanostructure width and largest height shows the highest performance. It suggests that smaller nanostructures with higher aspect ratio are favorable for high performance solar cells. The simple factor IEF in eq 1 can be used to illustrate the synergistic effects of width and height. As shown in Figure 3c and d, the increase of IEF generates constant increases of J_{sc} and PCE, which highlights the importance of a large PCPDTBT/C_{70} interfacial area. In this work. the average PCE of D6 (5.5%) is more than twice of that of D1 (~2.1%) and similar to the efficiency record people have made on this polymer (5.5%) when using the BHJ structure.[28] It therefore demonstrates that NIL can produce highly efficient low bandgap polymer solar cells through the well-ordered heterojunction when the nanostructure geometry is carefully optimized. It should also be noted that despite considerable effort, the highest PCEs obtained from nanoimprinted P3HT solar cells in literature are limited to approximately 3−4%, which are lower than the highest values (~4−5%) when the same polymer is used in the BHJ structure. It therefore indicates that NIL works better for low bandgap polymer solar cells. One possible explanation is that the method of using thermal or solvent vapor annealing to control the phase separation in P3HT based BHJ solar cells is very effective, as proven by a number of studies; while that of using additives in the low bandgap polymer solar cells is not, as described in literature.[28] This less effective approach leaves NIL more space to demonstrate its advantage in improving the solar cell performance when compared to the BHJ structure. This is our preliminary thinking and more studies are required to understand these different behaviors. Here, we believe a higher performance can be expected if one can further decrease the PCPDTBT nanostructure width while maintaining a large height, that is, increasing IEF. There is a large room to improve our device performance, as the largest IEF in D6 is less than 3.5. For different nanostructures with the same IEF, it seems that decreasing width can have a more positive impact than increasing height because the former can enhance the exciton dissociation and charge transport simultaneously. Our future work will focus on confirming these speculations experimentally.

4. CONCLUSION

In this work, we demonstrate the feasibility of using NIL to make well-ordered and efficient low bandgap polymer solar cells. High quality PCPDTBT nanogratings are fabricated using this technique for the first time. To study the nanostructure geometry effect, PCPDTBT/C_{70} solar cells with different feature sizes of PCPDTBT gratings are fabricated. It is found that the PCE increases with the decrease of nanostructure width, increase of height and IEF. A NIL improved chain ordering is observed as well. Devices with the highest PCE of ~5.5% are made on the highest aspect ratio PCPDTBT nanostructures, which is attributed to efficient charge separation, transport, and light absorption.

AUTHOR INFORMATION

Corresponding Author

*E-mail: walter.hu@utdallas.edu.

Notes

The authors declare no competing financial interest.

ACKNOWLEDGMENTS

This work is supported by National Science Foundation (NSF) (grant No. ECCS-0901759), Welch Foundation Grant AT-1617, and DOE Phase II STTR program on "Tandem Organic Solar Cells" (grant No. DE-SC00003664). The authors gratefully acknowledge M. Stefan from Department of Chemistry, J. Hsu from Department of Materials Science and Engineering and P. Zang from Department of Electrical Engineering at UT Dallas for their supports and helpful discussions.

REFERENCES

(1) Lewis, N. S. Toward Cost-Effective Solar Energy Use. *Science* **2007**, *315*, 798−801.

(2) Service, R. F. Outlook Brightens for Plastic Solar Cells. *Science* **2011**, *332*, 293−293.

(3) Haugeneder, A.; Neges, M.; Kallinger, C.; Spirkl, W.; Lemmer, U.; Feldmann, J.; Scherf, U.; Harth, E.; Gugel, A.; Mullen, K. Exciton Diffusion and Dissociation in Conjugated Polymer Fullerene Blends and Heterostructures. *Phys. Rev. B* **1999**, *59*, 15346−15351.

(4) Kroeze, J. E.; Savenije, T. J.; Vermeulen, M. J. W.; Warman, J. M. Contactless Determination of the Photoconductivity Action Spectrum, Exciton Diffusion Length, and Charge Separation Efficiency in Polythiophene-Sensitized TiO_2 Bilayers. *J. Phys. Chem. B* **2003**, *107*, 7696−7705.

(5) Yu, G.; Gao, J.; Hummelen, J. C.; Wudl, F.; Heeger, A. J. Polymer Photovoltaic Cells: Enhanced Efficiencies via a Network of Internal Donor−Acceptor Heterojunctions. *Science* **1995**, *270*, 1789−1791.

(6) Li, G.; Shrotriya, V.; Huang, J. S.; Yao, Y.; Moriarty, T.; Emery, K.; Yang, Y. High-Efficiency Solution Processable Polymer Photovoltaic Cells by Self-Organization of Polymer Blends. *Nat. Mater.* **2005**, *4*, 864−868.

(7) Ma, W. L.; Yang, C. Y.; Gong, X.; Lee, K.; Heeger, A. J. Thermally Stable, Efficient Polymer Solar Cells with Nanoscale Control of the Interpenetrating Network Morphology. *Adv. Funct. Mater.* **2005**, *15*, 1617−1622.

(8) Watkins, P. K.; Walker, A. B.; Verschoor, G. L. B. Dynamical Monte Carlo Modelling of Organic Solar Cells: The Dependence of Internal Quantum Efficiency on Morphology. *Nano Lett.* **2005**, *5*, 1814−1818.

(9) Yang, Y.; Mielczarek, K.; Aryal, M.; Zakhidov, A.; Hu, W. Nanoimprinted Polymer Solar Cell. *ACS Nano* **2012**, *6*, 2877−2892.

(10) Aryal, M.; Buyukserin, F.; Mielczarek, K.; Zhao, X.; Gao, J.; Zakhidov, A.; Hu, W. Imprinted Large-Scale High Density Polymer Nanopillars for Organic Solar Cells. *J. Vac. Sci. Technol., B* **2008**, *26*, 2562−2566.

(11) Aryal, M.; Trivedi, K.; Hu, W. Nano-Confinement Induced Chain Alignment in Ordered P3HT Nanostructures Defined by Nanoimprint Lithography. *ACS Nano* **2009**, *3*, 3085−3090.

(12) He, X.; Gao, F.; Tu, G.; Hasko, D.; Huettner, S.; Steiner, U.; Greenham, N. C.; Friend, R. H.; Huck, W. T. S. Formation of

Nanopatterned Polymer Blends in Photovoltaic Devices. *Nano Lett.* **2010**, *10*, 1302−1307.
(13) Yang, Y.; Aryal, M.; Mielczarek, K.; Hu, W.; Zakhidov, A. Nanoimprinted P3HT/C_{60} Solar Cells Optimized by Oblique Deposition of C_{60}. *J. Vac. Sci. Technol., B* **2010**, *28*, C6M104−C6M107.
(14) Tomohiro, K.; Tada, K.; Ishikawa, M.; Fujita, H.; Nishikura, N.; Kawata, H.; Hirai, Y. Novel Heterostructured Organic Photovoltaics Formed by Multilayered Direct Nanoimprinting. *Jpn. J. Appl. Phys.* **2013**, *52*, 06GJ03.
(15) Hlaing, H.; Lu, X.; Hofmann, T.; Yager, K. G.; Black, C. T.; Ocko, B. M. Nanoimprint-Induced Molecular Orientation in Semiconducting Polymer Nanostructures. *ACS Nano* **2011**, *5*, 7532−7538.
(16) He, X.; Gao, F.; Tu, G.; Hasko, D. G.; Huettner, S.; Greenham, N. C.; Steiner, U.; Friend, R. H.; Huck, W. T. S. Formation of Well-Ordered Heterojunctions in Polymer: PCBM Photovoltaic Devices. *Adv. Funct. Mater.* **2011**, *21*, 139−146.
(17) Johnston, D. E.; Yager, K. G.; Hlaing, H.; Lu, X.; Ocko, B. M.; Black, C. T. Nanostructured Surfaces Frustrate Polymer Semiconductor Molecular Orientation. *ACS Nano* **2013**, *8*, 243−249.
(18) Wiedemann, W.; Sims, L.; Abdellah, A.; Exner, A.; Meier, R.; Musselman, K. P.; MacManus-Driscoll, J. L.; Mueller-Buschbaum, P.; Scarpa, G.; Lugli, P.; Schmidt-Mende, L. Nanostructured Interfaces in Polymer Solar Cells. *Appl. Phys. Lett.* **2010**, *96*, 263109.
(19) Shih, C. F.; Hung, K. T.; Wu, J. W.; Hsiao, C. Y.; Li, W. M. Efficiency Improvement of Blended Poly(3-hexylthiophene) and 1-(3-methoxycarbonyl)-propyl-1-phenyl-(6,6)C_{61} Solar Cells by Nanoimprinting. *Appl. Phys. Lett.* **2009**, *94*, 143505.
(20) Zhou, M.; Aryal, M.; Mielczarek, K.; Zakhidov, A.; Hu, W. Hole Mobility Enhancement by Chain Alignment in Nanoimprinted Poly(3-hexylthiophene) Nanogratings for Organic Electronics. *J. Vac. Sci. Technol., B* **2010**, *28*, C6M63−C66M67.
(21) Chen, D.; Zhao, W.; Russell, T. P. P3HT Nanopillars for Organic Photovoltaic Devices Nanoimprinted by AAO Templates. *ACS Nano* **2012**, *6*, 1479−1485.
(22) Liu, Y.; Kirsch, C.; Gadisa, A.; Aryal, M.; Mitran, S.; Samulski, E. T.; Lopez, R. Effects of Nano-Patterned versus Simple Flat Active Layers in Upright Organic Photovoltaic Devices. *J. Phys. D: Appl. Phys.* **2013**, *46*, 024008.
(23) Li, G.; Zhu, R.; Yang, Y. Polymer Solar Cells. *Nat. Photonics* **2012**, *6*, 153−161.
(24) Park, S. H.; Roy, A.; Beaupre, S.; Cho, S.; Coates, N.; Moon, J. S.; Moses, D.; Leclerc, M.; Lee, K.; Heeger, A. J. Bulk Heterojunction Solar Cells with Internal Quantum Efficiency Approaching 100%. *Nat. Photonics* **2009**, *3*, 297−302.
(25) Koppe, M.; Egelhaaf, H.-J.; Dennler, G.; Scharber, M. C.; Brabec, C. J.; Schilinsky, P.; Hoth, C. N. Near IR Sensitization of Organic Bulk Heterojunction Solar Cells: Towards Optimization of the Spectral Response of Organic Solar Cells. *Adv. Funct. Mater.* **2010**, *20*, 338−346.
(26) Liang, Y.; Xu, Z.; Xia, J.; Tsai, S.-T.; Wu, Y.; Li, G.; Ray, C.; Yu, L. For the Bright Future-Bulk Heterojunction Polymer Solar Cells with Power Conversion Efficiency of 7.4%. *Adv. Mater.* **2010**, *22*, E135−E138.
(27) Fischer, F. S. U.; Tremel, K.; Saur, A. K.; Link, S.; Kayunkid, N.; Brinkmann, M.; Herrero-Carvajal, D.; Navarrete, J. T. L.; Delgado, M. C. R.; Ludwigs, S. Influence of Processing Solvents on Optical Properties and Morphology of a Semicrystalline Low Bandgap Polymer in the Neutral and Charged States. *Macromolecules* **2013**, *46*, 4924−4931.
(28) Peet, J.; Kim, J. Y.; Coates, N. E.; Ma, W. L.; Moses, D.; Heeger, A. J.; Bazan, G. C. Efficiency Enhancement in Low-Bandgap Polymer Solar Cells by Processing with Alkane Dithiols. *Nat. Mater.* **2007**, *6*, 497−500.
(29) Liao, H.-C.; Ho, C.-C.; Chang, C.-Y.; Jao, M.-H.; Darling, S. B.; Su, W.-F. Additives for Morphology Control in High-Efficiency Organic Solar Cells. *Mater. Today* **2013**, *16*, 326−336.
(30) Lee, J. K.; Ma, W. L.; Brabec, C. J.; Yuen, J.; Moon, J. S.; Kim, J. Y.; Lee, K.; Bazan, G. C.; Heeger, A. J. Processing Additives for Improved Efficiency from Bulk Heterojunction Solar Cells. *J. Am. Chem. Soc.* **2008**, *130*, 3619−3623.
(31) Gu, Y.; Wang, C.; Russell, T. P. Multi-Length-Scale Morphologies in PCPDTBT/PCBM Bulk-Heterojunction Solar Cells. *Adv. Energy Mater.* **2012**, *2*, 683−690.
(32) Lin, R.; Wright, M.; Uddin, A. Effects of Solvent Additive on Inverted Structure PCPDTBT:PC_{71}BM Bulk Heterojunction Organic Solar Cells. *Physica Status Solidi A* **2013**, *210*, 1785−1790.
(33) Scharber, M. C.; Lungenschmied, C.; Egelhaaf, H.-J.; Matt, G.; Bednorz, M.; Fromherz, T.; Gao, J.; Jarzab, D.; Loi, M. A. Charge Transfer Excitons in Low Band Gap Polymer based Solar Cells and the Role of Processing Additives. *Energy Environ. Sci.* **2011**, *4*, 5077−5083.
(34) Cheyns, D.; Vasseur, K.; Rolin, C.; Genoe, J.; Poortmans, J.; Heremans, P. Nanoimprinted Semiconducting Polymer Films with 50 nm Features and Their Application to Organic Heterojunction Solar Cells. *Nanotechnology* **2008**, *19*, 424016.
(35) Zeng, W.; Chong, K. S. L.; Low, H. Y.; Williams, E. L.; Tam, T. L.; Sellinger, A. The Use of Nanoimprint Lithography to Improve Efficiencies of Bilayer Organic Solar Cells based on P3HT and a Small Molecule Acceptor. *Thin Solid Films* **2009**, *517*, 6833−6836.
(36) Yang, Y.; Lee, K.; Mielczarek, K.; Hu, W.; Zakhidov, A. Nanoimprint of Dehydrated PEDOT:PSS for Organic Photovoltaics. *Nanotechnology* **2011**, *22*, 485301.
(37) Zhong, Z. W.; Shan, X. C.; Yao, Y. C. Investigation of Antiadhesive Coatings for Nanoimprinting Lithography. *Mater. Manuf. Processes* **2010**, *25*, 658−664.
(38) Pfuetzner, S.; Meiss, J.; Petrich, A.; Riede, M.; Leo, K. Improved Bulk Heterojunction Organic Solar Cells Employing C_{70} Fullerenes. *Appl. Phys. Lett.* **2009**, *94*, 223307−223303.
(39) Lee, J. H.; Kim, D. W.; Jang, H.; Choi, J. K.; Geng, J.; Lung, J. W.; Yoon, S. C.; Jung, H.-T. Enhanced Solar-Cell Efficiency in Bulk-Heterojunction Polymer Systems Obtained by Nanoimprinting with Commercially Available AAO Membrane Fitters. *Small* **2009**, *5*, 2139−2143.
(40) Di Nuzzo, D.; Aguirre, A.; Shahid, M.; Gevaerts, V. S.; Meskers, S. C. J.; Janssen, R. A. J. Improved Film Morphology Reduces Charge Carrier Recombination into the Triplet Excited State in a Small Bandgap Polymer-Fullerene Photovoltaic Cell. *Adv. Mater.* **2010**, *22*, 4321−4324.
(41) Kline, R. J.; McGehee, M. D.; Toney, M. F. Highly Oriented Crystals at the Buried Interface in Polythiophene Thin-Film Transistors. *Nat. Mater.* **2006**, *5*, 222−228.
(42) Chang, J.-F.; Sun, B.; Breiby, D. W.; Nielsen, M. M.; Sölling, T. I.; Giles, M.; McCulloch, I.; Sirringhaus, H. Enhanced Mobility of Poly(3-hexylthiophene) Transistors by Spin-Coating from High-Boiling-Point Solvents. *Chem. Mater.* **2004**, *16*, 4772−4776.
(43) Yamamoto, K.; Ochiai, S.; Wang, X.; Uchida, Y.; Kojima, K.; Ohashi, A.; Mizutani, T. Evaluation of Molecular Orientation and Alignment of Poly(3-hexylthiophene) on Au (111) and on Poly(4-vinylphenol) Surfaces. *Thin Solid Films* **2008**, *516*, 2695−2699.